C.E. SACLAY
DSM

SERVICE DE PHYSIQUE NUCLÉAIRE

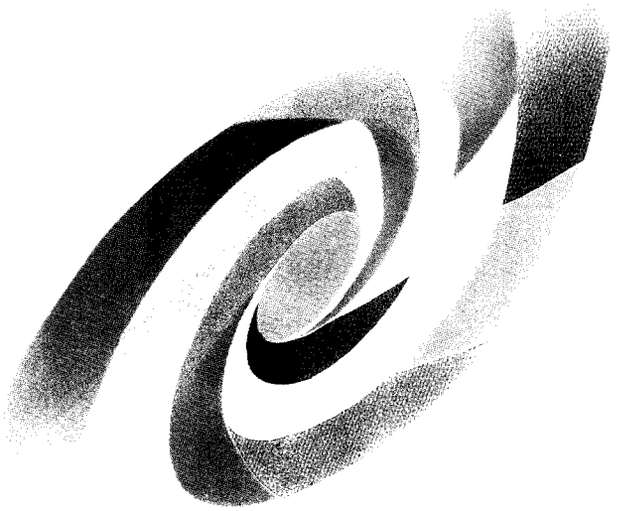

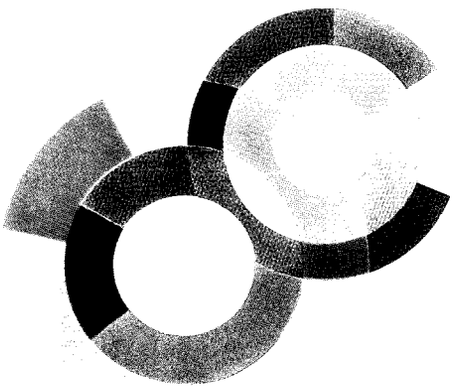

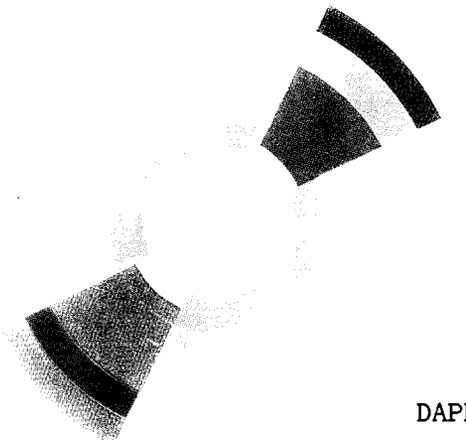

DAPNIA/SPhN 93 64 12/1993

TWO-BODY PHOTODISINTEGRATION OF ^{3}He BETWEEN 200 AND 800 MeV

V. Isbert, G. Audit, N. d'Hose,
S. Kerhoas, M. Mac Cormick,
L.Y. Murphy, G. Tamas, S. Altieri,
A. Braghieri, P. Pedroni, T. Pinelli,
J. Ahrens, R. Beck, J. Peise,
J.R.M. Annand, R. Crawford

DAPNIA

Le DAPNIA (**D**épartement d'**A**strophysique, de physique des **P**articules, de physique **N**ucléaire et de l'**I**nstrumentation **A**ssociée) regroupe les activités du Service d'Astrophysique (SAp), du Département de Physique des Particules Elémentaires (DPhPE) et du Département de Physique Nucléaire (DPhN).

Adresse : DAPNIA, Bâtiment 141
CEA Saclay
F - 91191 Gif-sur-Yvette Cedex

Two Body Photodisintegration of ^{3}He Between 200 And 800 MeV

V. Isbert *, G. Audit, N. d'Hose, S. Kerhoas, M. Mac Cormick, L.Y. Murphy, G. Tamas
SPhN-DAPNIA, C.E.N. Saclay, 91191 Gif sur Yvette, France

S. Altieri[a,b], A. Braghieri[a,b †], P. Pedroni[a], T. Pinelli[a,b]
[a] *INFN-Sezione di Pavia, via Bassi 6, 27100 Pavia, Italy*
[b] *Dipartimento di Fisica Nucleare e Teorica, Università degli Studi di Pavia, via Bassi 6, 27100 Pavia, Italy*

J. Ahrens, R. Beck, J. Peise
Institut für Kernphysik, Universität Mainz, 55099 Mainz, Germany

J.R.M. Annand, R. Crawford
Kelvin Laboratory, University of Glasgow, UK

Abstract

Differential cross sections for the ^{3}He(γ, pd) reaction at photon energies between 200 and 800 MeV at all proton c.m. angles between 35° and 145° have been measured using the tagged photon beam facility of the 855 MeV MAMI accelerator in Mainz. Reaction products were detected using the large acceptance detector DAPHNE. The results confirm the rapid decrease of forward angles cross sections with increasing E_γ whilst at backward angles, aided by the high precision of the measurement, we can see a clear enhancement in the angular distribution which is a possible signature of three-body mechanisms.

NUCLEAR REACTIONS ^{3}He(γ, pd) ; E_γ from 200 to 800 MeV ; θ_p^{cm} from 35° to 145° ; measured $d\sigma/d\Omega\,(E_\gamma)$ at fixed θ_p^{cm} and $d\sigma/d\Omega\,(\theta_p^{cm})$ at fixed E_γ

Correspondence to: Dr. P. Pedroni, INFN-Sezione di Pavia, via Bassi 6, 27100 Pavia, Italy
*present address *Institut für Kernphysik, Universität Mainz, 55099 Mainz, Germany*
†present address *SPhN-DAPNIA, C.E.N. Saclay, France*

1. Introduction

Photodisintegration processes via one nucleon photoabsorption are strongly suppressed at medium energies due to momentum mismatch and these reactions are correspondingly sensitive to two and three-body photoabsorption mechanisms. For this reason, the study of $\gamma\,^3\mathrm{He} \rightarrow pd$ and $\gamma^3\mathrm{He} \rightarrow ppn$ reactions over a large energy and momentum domain provides an unique opportunity to investigate in detail these mechanisms.

In particular, it was suggested that the $\gamma\,^3\mathrm{He} \rightarrow pd$ reaction is dominated at forward angles by two body mechanisms [1,2] whilst at backward angles it is dominated by three-body processes [2].

There have already been several experiments designed to measure this reaction [3–6] in which the main interest has been to study the principle of 'time reversal invariance' (TRI) with respect to $pd \rightarrow \gamma\,^3\mathrm{He}$. However, these experiments were limited in energy range, all being carried out at $E_\gamma \leq$ 550 MeV, and only two excitation curves, at $\theta_p^{cm} = 60°$ and at $\theta_p^{cm} = 90°$, have been obtained. In addition, two experiments at Caltech [4] and Bonn [5] have measured some angular distributions.

The recent developments in 100% duty cycle accelerators, used in conjunction with large angular and momentum acceptance detectors, provide the possibility of completing the study of two and three-body ^{3}He photodisintegration at intermediate energies ($E_\gamma < 1$ GeV).

In this paper we present the results obtained for the $^3\mathrm{He}(\gamma, pd)$ reaction using the large acceptance detector DAPHNE [7] in conjunction with the tagged photon beam facility installed at the MAMI accelerator at the University of Mainz [8].

A total of 1.7×10^5 events were recorded from this reaction during a period of four days. The photon energy range was 200–800 MeV and the c.m. polar angular coverage $35° - 145°$.

2. The Experimental Set-Up

2.1. THE PHOTON BEAM

DAPHNE is associated with the tagged photon facility installed at the 855 MeV continuous wave electron accelerator MAMI in Mainz. The photons are obtained by bremsstrahlung of the primary beam through a very thin radiator (3×10^{-4} radiation lengths). A magnetic spectrometer with a 352-scintillators focal plane counter enables photon tagging from 50-800 MeV with a resolution of the order of 2 MeV [9]. Losses due to collimation of the photon beam gave an experimental tagging efficiency (the probability of a tagged photon entering the interaction target given an electron hit on the focal plane) of about 55%. The number of photons was continuously monitored with a simple pair detector (a thin copper converter followed by two scintillators located downstream of DAPHNE) which counted in coincidence with the tagger. The photon detection efficiency of this device was repeatedly measured, throughout the data acquisition period, at low beam intensity, by comparison with a 100% efficient lead-glass detector (25 cm $\times$ 25 cm $\times$ 25 cm). The absolute normalisation uncertainty is estimated to be equal to 2%.

2.2. DAPHNE

DAPHNE (Detecteur à grande Acceptance pour la PHysique photoNucleaire Experimentale) is a 3.7π acceptance hadron detector which has been developed by the INFN, sezione di Pavia, and the SPhN-DAPNIA of Saclay. This device has a central tracking detector, consisting of three coaxial cylindrical multiwire proportional counters, surrounded by a segmented cylindrical scintillator ΔE-E telescope for charged particle identification. Finally there is a scintillator-absorber sandwich that is designed to enhance the π° detection efficiency. A detailed description is given in ref.[7] and its experimental

performance is reported in ref.[10].

The trigger is very simple, activated by a coincidence between two charged particles in DAPHNE and one tagger channel. Events with charged pions in the final state were reduced by the choice of an appropriate electronic threshold.

Particle detection thresholds determine a lower photon energy limit of 200 MeV for ^{3}He(γ, pd) measurements. An integrated tagged photon beam intensity of $\sim\ 3 \times 10^6\ \gamma$/s for $200 \leq E_\gamma \leq 800$ MeV produced a trigger rate of $\sim$ 100 Hz.

2.3. THE ^{3}He TARGET

Liquid ^{3}He at 2.65 K and 556 mbar is contained in a Mylar cylinder of dimensions 4.3 cm diameter by 27.5 cm length with a wall thickness of 0.1 mm. Liquifaction was obtained with a Gifford-MacMahon ^{4}He refrigerator coupled to a Joule-Thomson expansion valve which provides the pressure reduction necessary (0.12 mbar) in order to reach this low temperature. The cryogenic system was automatically regulated and all critical parameters relating to the target environment were continuously recorded [11]. During the operating conditions, the stability in temperature reached 5×10^{-3} K. This ensured a stability in the target density of the order of 0.5 %.

3. Data Analysis

Thanks to the high resolution of the DAPHNE tracking section, the interaction vertex of the events with two charged particles in the final state can be reconstructed with great precision [7]. Software cuts on the vertex coordinates allow a complete suppression of events originating in the target walls and therefore we had no need to correct ^{3}He data for empty target contributions.

In order to completely determine the kinematics associated with a two-body reaction we must measure the photon energy, the angles of the two particles and determine the nature of at least one of them.
Putting aside the subtraction of accidental coincidences (which are always less than 1%), data reduction to selected events of interest may be divided into three parts:

a) the angular analysis,

b) particle identification,

c) background subtraction.

3.1. DATA REDUCTION BASED ON THE ANGULAR INFORMATION

Figure 1 shows the number of events for two charged particles versus the angular difference $\Delta\phi = (\phi_2^{exp} - \phi_1^{exp} - \pi)$ where ϕ_1^{exp} and ϕ_2^{exp} are the azimuthal angles of the two outgoing particles and $\phi_2^{exp} > \phi_1^{exp}$. A pronounced peak appears clearly around $\Delta\phi = 0$. This peak contains all coplanar events which characterise the two-body reactions of interest. We have applied a first cut ($\mid \Delta\phi \mid < 0.1$ rad), as shown by the double hatched area of figure 1, in order to reject the largest part of the contamination processes. This window in ϕ is much wider than the DAPHNE azimuthal resolution.

Let us now consider the correlation between the polar angles of the two particles. Given the polar angle of the first particle θ_1^{exp}, and the initial photon energy, we can calculate the polar angle of the second particle, θ_2^{theo}. Since, as yet, the nature of the particle is unknown we calculate θ_2^{theo} for each of the two possible cases (ie. proton, deuteron). We evaluate the difference $\Delta\theta_{p(d)} = (\theta_2^{exp} - \theta_2^{theo})$ for the two cases and take the correct value as the one closest to zero. Figure 2 shows the number of events versus $\Delta\theta_{min} = \mathrm{Min}\{\Delta\theta_p, \Delta\theta_d\}$. The peak corresponding to *pd* events shows up clearly over a background corresponding to all other reactions that have at least two charged particles in the final state (eg. ppn, $pp\pi^-$). As the $\Delta\theta$ correlations for quasifree photoproduction processes (eg. $\gamma\,{}^3\mathrm{He} \rightarrow p\pi^- + (pp)_{spectator}$) are completely different to the $\gamma({}^3\mathrm{He}, pd)$ case, such processes do not appear within the range of figure 2.

Applying two cuts, one in $\Delta\phi$ and the other in $\Delta\theta$, is enough to isolate the *pd* events. There remains a background due to three-body final state events which can be determined for $\mid \Delta\phi \mid > 0.1$ rad and, consequently, subtracted.

In order to extract a differential cross section from the remainder we must identify the particles as being either protons or deuterons. Unfortunately, this cannot be done by angular analysis alone. If we invert the role of the two particles, the $\Delta\theta$ correlation does not change significantly. For example, at $E_\gamma = 300$ MeV:

$$\begin{array}{rcl@{\qquad}rcl} \theta_{proton} & = & 60^\circ & \theta_{deuteron} & = & 93.02^\circ \\ \theta_{deuteron} & = & 60^\circ & \theta_{proton} & = & 94.12^\circ \end{array}$$

Since the experimental angular resolution does not allow us to make a choice between these two possibilities, we need to identify at least one of the particles.

3.2. PARTICLE IDENTIFICATION

Particle identification is obtained by comparison of the measured (from pulse height) and the expected values of the particles' kinetic energies.

We fit the experimental dE/dx information with the known energy-loss curves for the proton and the deuteron in order to reconstruct the particle's initial kinetic energy. Since the nature of the particle is as yet unknown, we calculate, event by event, two different sets of values:

$$\left(E_p^{exp}\,;\,E_d^{exp}\right)_{p,d(d,p)}$$

with the subscript p,d (d,p) corresponding to the case in which the first particle detected was a proton (deuteron) and the second one a deuteron (proton).

In addition, we can use the known photon energy and the angle of each emitted particle to obtain the expected value of its kinetic energy, E^{theo}, using the constraints of two-body kinematics. Thus, we again have two different sets of values

$$\left(E_p^{theo}\,;\,E_d^{theo}\right)_{p,d(d,p)}$$

where the subscript corresponds, as before, to the proton-deuteron (deuteron-proton) configuration. If we now calculate the difference $\Delta E = |E^{theo} - E^{exp}|$ we get four ΔE values:

$$\left(\Delta E_p\,;\,\Delta E_d\right)_{p,d(d,p)}$$

two for each configuration. The "correct" configuration is taken as the one having the lowest value of ΔE. This allows us to positively identify, in nearly all events, at least one of the particles. The other one may (or may not) have undergone a nuclear interaction in the detector, which tends to reduce the pulse height signal.

This identification method is extremely efficient as long as the particles stop in the detector since the resolution $\Delta E/E$ (FWHM) of the reconstructed kinetic energy is quite good. For protons, it is about 6% in

the energy range 50–200 MeV [10]. However, when the particles do not stop in the detector the resolution is poorer and the scintillators information can be ambiguous as the full energy signal is not obtained. In order to maintain good discrimination we applied a cut on the deuteron kinetic energy $(E_d^{exp} - E_d^{theo})/E_d^{theo} < 20\%$ which avoids any ambiguity in the discrimination between protons and deuterons. This upper limit on E_d^{exp}, which conserves the deuterons which have undergone a nuclear interaction, produces a detection inefficiency dependent only on the experimental resolution. Using the measured scintillators resolution, the response of DAPHNE was modelled using the GEANT code [12] in order to quantify the loss of efficiency. Figure 3a shows the comparison between simulation and experiment for a deuteron energy of 120 MeV where the statistics are good. The agreement is excellent and this gives us confidence in the calculation of the correction.

Background coming from events with two charged baryons and a pion in the final state (eg. $pp\pi^-$, $pd\pi^\circ$) was reduced by applying an additional condition, $E_p^{theo} - E_p^{exp} < 100$ MeV, such difference being less than the mass of a pion. This limit cuts out part of the tail due to secondary proton nuclear interactions and the corresponding loss of efficiency was evaluated, including in the GEANT code, the hadronic proton cross-sections for the detector materials. It has been shown [13] that the protons' nuclear interactions are well calculated and a comparison between the simulation and the experiment for a proton energy of 200 MeV is shown in figure 3b.

The effect of these selections on the simulated response to protons and deuterons is shown in figure 4. A constant isotropic cross section was assumed for the calculation. These two cuts introduce a correction ranging from $\sim$ 1% at $E_\gamma = 200$ MeV, $\theta_d^{lab} = 30^\circ$, to 42% at $E_\gamma = 800$ MeV, $\theta_d^{lab} = 150^\circ$ (see fig. 5). The loss of events where both the proton and the deuteron have had a nuclear interaction has also to be evaluated. This cal-

culation gives the main contribution to the systematic error of the analysis because in the case of the deuteron the GEANT code underestimates the nuclear interaction tail, as it is also manifested in figure 3a. From the comparison between the simulated and the experimental response we estimate, depending to photon energy, the overall systematic error in the cross section evaluation to be ranging from 1% to 5%, due to the particle identification method.

3.3. BACKGROUND SUBTRACTION

The final remaining background, due mainly to *ppn* events, is suppressed by reworking the entire analysis process but with the initial condition taken as

$$0.1 < \mid \Delta\phi \mid \leq 0.2\,\text{rad}.$$

For the *ppn* case a shift of 0.1 rad in $\Delta\phi$ corresponds to a 5 MeV/c shift in momentum for a 1 GeV/c proton and the reasonable assumption is that the *ppn* cross-section is constant within the $\Delta\phi$ shift.

Figure 6 shows the final selection for *pd* events (white area) and background events (hatched area). The background substraction ranges from 3% at $E_\gamma = 250$ MeV, $\theta_p^{cm} = 45°$, to 70% at $E_\gamma = 750$ MeV, $\theta_p^{cm} = 135°$.

3.4. CROSS SECTION EVALUATION

The differential cross-section, for a fixed E_γ and θ bin, is given by:

$$\frac{d\sigma}{d\Omega} = \frac{1}{\epsilon} \cdot \frac{N_{pd}(E_\gamma, \theta)}{N_\gamma(E_\gamma) \cdot N_{targ}} \cdot \frac{1}{2\pi \sin\theta d\theta}$$

where $N_{pd}(E_\gamma, \theta)$, $N_\gamma(E_\gamma)$ and N_{targ} are respectively the number of *pd* events and of photons in the selected bin and the number of target nuclei per cm^2. $N_{pd}(E_\gamma, \theta)$ is corrected, event by event, for geometrical effects due to the target extension and for the inefficiency of the particle identification method.

The factor ϵ includes the correction due to the inefficiency of recontruction of the tracks by the vertex detector. This parameter was measured both by using cosmic rays and by selecting, among the recorded experimental data, only those events for which clear and unambiguous signals were detected in the scintillators. We found that, in the case of two coincident charged particles, $\epsilon = 96\%$ with a systematic error of 1%.

All the systematic errors accounted for in the evaluation of the cross section are summarized in table 1.

4. Results and Comments

The kinematical domain accessible in this experiment is defined by an upper energy limit (800 MeV) which corresponds to the maximum energy of the tagged photon beam and a lower limit (200 MeV) which is set by the hadron detection threshold. The angular acceptance of DAPHNE for two coincident charged particles gives the c.m. angular range for protons.

We present in figs. 7 and 8 the subset of our data which were taken under the kinematical conditions of previously published data.

a) Figure 7 shows excitation functions at $\theta_p^{cm} = 60°$ and $\theta_p^{cm} = 90°$. Our results at $\theta_p^{cm} = 90°$ are in agreement with those of MIT [6], which were taken at $E_\gamma \leq 340$ MeV, while at $\theta_p^{cm} = 60°$ our data are roughly 15% lower. We recall that the MIT experiment was the last one carried out for the measurement of the γ^3He $\rightarrow pd$ reaction and that much effort was made to reduce the systematic errors. [‡]

However, we would like to stress that all our data were recorded simultaneously under the same experimental conditions. For this reason, the distortion between the two different kinematical conditions shown is negligible. The overall systematic errors are also minimized (see table 1).

This was not the case in the previous experiments. All used untagged bremsstrahlung beams that did not allow accurate photon flux measurement. Comparing the results obtained in Saclay [3], Caltech [4], Bonn [5], and MIT it is clear that systematic errors are very large.

b) Figure 8 presents seven angular distributions at E_γ =267, 326, 420, 450, 500, 550 and 650 MeV, where our data are compared with those of Bonn (up to 420 MeV) and Caltech (up to 550 MeV). Certainly,

[‡]Comparison of the MIT data with the most recent inverse reaction measurements $pd \rightarrow \gamma^3$He [14], [15] gave no evidence of TRI violation.

for $E_\gamma < 500$ MeV, where the previous differential cross-sections are relatively well defined, there are significant differences in the angular distributions. Again, we have to notice that the present data are not subject to the errors in the cross-section normalisation inherent to the older measurements.

Our entire data set is summarised in table 2 and is shown in figure 9.

In agreement with the previous data we measure a rapid, monotonic decrease in excitation functions (see figure 7) in contrast to the deuteron photodisintegration where a Δ-excitation bump is clearly seen. For ^{3}He(γ, pd) this process is suppressed by the influence of the form factor linked to the formation of a deuteron in the final state, as was previously demonstrated by Maximon and Prats [1] and Laget [2]. The differential cross-sections show, at a fixed E_γ, a steep decrease up to $\theta_p^{cm} \simeq 90°$, due to the dominance of the two-body photodisintegration mechanisms [1,2].

At backward angles, where the present data should certainly be superior to previous measurements, a bump in the differential cross-section is observed. This is precisely the region where three-body mechanisms are expected to be important [2]. The most up-to-date calculations of Laget (see appendix A) are compared to the data, for different values of E_γ, in figure 8. In all cases, the dashed curve gives the contribution of the one and two-body mechanisms (diagrams A of figure 10), while the full line also includes the 3-body mechanisms shown in diagram B. It is evident that at backward angles the one and two-body mechanisms are not sufficient to reproduce either the magnitude or the form of the cross section. The inclusion of the 3-body process clearly results in overestimation of the data, whilst the qualitative form of the cross section is roughly reproduced. This discrepancy may be attributed to the different approximations contained in the treatment of the associated terms:

a) the absorption of a pion by an isoscalar nucleon pair is about six times

larger than the absorption by an isovector nucleon pair. In the calculation, only the absorption of the intermediate pion (diagram B) by a T=0 pair was taken into account. In this case the formation of a Δ at the photoproduction vertex is forbidden, since the total isospin of the *pd* final state is T=$\frac{1}{2}$. However, if the pion is absorbed by a T=1 pair the Δ can be excited at the photoproduction vertex and the resulting amplitude, which might contribute significantly, is not taken into account.

b) The double pion photoproduction mechanism (diagram C), that may play an important role when $E_\gamma > 450$ MeV, is not included.

c) The Fermi motion of the nucleon at the photonuclear vertex is not taken into account for the 3-body terms as it requires the manipulation of a nine-dimensional integral (on the other hand it is fully introduced in the two-body amplitude).

5. Conclusions

For the first time the cross-section of the ^{3}He(γ, pd) reaction has been measured with monochromatic photons in a single experiment covering a wide energy and angular range.

At forward angles our excitation functions show little structure, confirming that the cross-section is dominated by the deuteron form factor which supresses the Δ photoproduction mechanism. However a structure indicative of three-body absorption mechanisms is clearly visible in the backward angle differential cross-sections. This data set provides a strong constraint on further theoretical studies on the role of the three-body processes.

Due to the different spin/isospin selection rules involved, this study complements that of the *ppn* reaction, which has also been measured and will appear in a future publication.

ACKNOWLEDGEMENTS

We would like to thank J.M. Laget for having provided us with the latest version of his calculations. We are grateful to K.H. Kaiser and the machine crew for all their hard work and the excellent beam quality that was maintained throughout the experiment. We wish also to acknowledge I. Antony, J.D. Kellie, S.J. Hall and G.J. Miller for the considerable assistance they provided the setting-up and maintenance of the photon tagging detector.

APPENDIX A

In [2], the m/E term in the relativistic expression for the nucleon propagator:

$$\frac{\gamma p + m}{p^2 - m^2} = \frac{m}{E}\frac{\overline{u}u}{p^\circ - E_\gamma} + \frac{m}{E}\frac{\overline{v}v}{p^\circ + E_\gamma}$$

was omitted.

It is taken into account in the calculations reported in this work. It amounts to a decrease of a factor $\sim$2 in the cross-section at backward angles.

References

[1] L.C. Maximon and F. Prats, Proc. Particle and Nuclei 10th Int. Conf., Heidelberg 1984; F. Prats, Phys. Lett. **B88** (1979) 23

[2] J.M. Laget, Phys. Rev. **C38** (1988) 2993

[3] P.E. Argan et al., Nucl. Phys. **A237** (1975) 447

[4] C.A. Heusch et al., Phys. Rev. Lett. **37** (1976) 405

[5] H.J. Gassen et al., Z. Phys. **A303** (1981) 35

[6] D.I. Sober et al., Phys. Rev. **C28** (1983) 2234

[7] G. Audit et al., Nucl. Instr. Meth. **A301** (1991) 473

[8] H. Herminghaus et al., Proc. 1990 Linear Accelerator Conf., Albuquerque 1990, preprint LA-12004-C ; Nucl. Instr. Meth. **A138** (1976) 1

[9] I. Anthony et al., Nucl. Instr. Meth. **A301** (1991) 230

[10] A. Braghieri et al., C.E.A. report DAPNIA-SPhN 93-48 (1993)

[11] B. Hervieu et al., Comptes Rendus des quatrièmes journeés d'Aussois, Aussois 1993, ed. CNRS Grenoble

[12] R. Brun et al., GEANT3 User Guide, CERN report DD/EE/84-1 (1987)

[13] P. Pedroni, INFN report BE-88/3 (1988)

[14] J.M. Cameron et al., Nucl. Phys. **A424** (1984) 549

[15] W.J. Briscoe et al., Phys. Rev. **C32** (1985) 1956

Figure captions

1. Distribution of two charged particle events versus the angular difference $\Delta\phi = (\phi_2^{exp} - \phi_1^{exp} - \pi)$ where ϕ_1^{exp} and ϕ_2^{exp} are the azimuthal angles of the outgoing particles and $\phi_2^{exp} > \phi_1^{exp}$. The double hatched area contains the coplanar events of the $\gamma^3\mathrm{He} \rightarrow pd$ reaction. Events in the hatched area were analysed in order to evaluate background contributions.

2. Distribution of two charged particle events having $\Delta\phi \leq 0.1$ rad versus the difference $\Delta\theta_{min} = \mathrm{Min}\{\Delta\theta_p, \Delta\theta_d\}$. The hatched area, that is selected by the condition $\Delta\theta \leq 0.07$ rad, contains the events from the $\gamma^3\mathrm{He} \rightarrow pd$ reaction.

3. The experimental response (circles) for (a) deuterons having a kinetic energy of 120 MeV at $\theta_{lab} = 90°$ and (b) for protons having a kinetic energy of 200 MeV at $\theta_{lab} = 90°$ is compared to the results of the simulation (continuous line).

4. Simulated distribution of the ratio $(E^{theo} - E^{exp})/E^{theo}$ versus E^{theo} for the two cases (a) deuteron and (b) proton. Events in (a) located on the left-hand side of the cut correspond to $(E_d^{theo} - E_d^{exp})/E_d^{theo} > 20\%$. The sparsely populated region on the right-hand side corresponds to the deuteron nuclear interactions. The region in (b) to the right-hand of the cut corresponds to $E_p^{theo} - E_p^{exp} > 100$ MeV.

5. Simulated efficiency of the particle identification method versus E_γ and θ_d^{lab}.

6. Shows the same distribution as figure 2 but for the events accepted in the particle identification analysis. The white (dark) area corresponds to events having $\Delta\phi \leq 0.1$ rad ($\Delta\phi > 0.1$ rad)

7. The excitation curves at $\theta_p^{cm} = 60°$ (a) and $\theta_p^{cm} = 90°$ (b) obtained in the present experiment are compared with the previous measurements.

8. Angular distributions at E_γ=267, 326, 420, 450, 500, 550 and 650 MeV, obtained in the present experiment are compared to the previously published data (up to 550 MeV) and to the theoretical calculations of Laget (ref.[2] and appendix A). The dashed curve gives the contribution of one and two-body mechanisms while the continuous curve include also the contribution of three-body processes.

9. Angular distributions at all the measured photon energies.

10. The relevant diagrams for the one-body, two-body (A) and three-body (B,C) mechanisms contributing to the γ^3He $\rightarrow pd$ reaction.

TABLE 1

Systematic errors

Number of photons	$\pm 2\,\%$
Target thickness	$\pm 0.5\,\%$
Wire chambers efficiency	$\pm 1\,\%$
Particle identification method (depending to photon energy)	$\pm 1\text{–}5\,\%$

TABLE 2

Differential cross sections $(d\sigma/d\Omega)$ (nb/sr) in the c.m. system for the ^{3}He(γ, pd) reaction, determined for 30 photon energy bins centered on the specified values of E_γ. The width of all the angular bins is $\pm 5°$ and the errors quoted are due to statistics only. There is an additional systematic uncertainty that ranges from $\pm 4.5\%$ at $E_\gamma = 205$ MeV to $\pm 8.5\%$ at $E_\gamma = 750$ MeV.

E_γ (MeV)	θ_p^{cm} (deg)										
	40°	50°	60°	70°	80°	90°	100°	110°	120°	130°	140°
205 ± 5		753 ± 15	604 ± 12	538 ± 10	437 ± 9	363 ± 8	285 ± 7	221 ± 7	162 ± 7	111 ± 6	67 ± 6
215 ± 5		702 ± 15	572 ± 12	471 ± 10	400 ± 9	302 ± 8	259 ± 7	203 ± 7	163 ± 7	108 ± 6	60 ± 6
225 ± 5		638 ± 15	529 ± 12	458 ± 10	346 ± 9	270 ± 8	215 ± 7	161 ± 7	130 ± 7	104 ± 7	52 ± 6
235 ± 5	790 ± 25	600 ± 15	514 ± 12	413 ± 10	329 ± 8	244 ± 7	197 ± 7	151 ± 6	120 ± 6	83 ± 6	48 ± 6
245 ± 5	616 ± 17	566 ± 13	467 ± 11	380 ± 9	282 ± 7	203 ± 6	160 ± 6	132 ± 5	96 ± 5	75 ± 5	53 ± 5
255 ± 5	592 ± 19	532 ± 15	449 ± 12	340 ± 10	255 ± 8	186 ± 7	137 ± 6	115 ± 6	73 ± 6	70 ± 6	40 ± 6
265 ± 5	520 ± 18	501 ± 15	430 ± 12	325 ± 10	240 ± 8	159 ± 7	123 ± 6	105 ± 6	85 ± 6	59 ± 6	44 ± 6
275 ± 5	479 ± 19	513 ± 17	378 ± 13	289 ± 10	213 ± 8	149 ± 7	108 ± 6	92 ± 6	72 ± 6	66 ± 7	50 ± 7
285 ± 5	510 ± 19	487 ± 16	362 ± 12	262 ± 9	194 ± 8	132 ± 6	95 ± 6	79 ± 6	70 ± 6	50 ± 6	46 ± 7
295 ± 5	432 ± 16	433 ± 14	330 ± 11	234 ± 8	162 ± 7	127 ± 6	93 ± 5	80 ± 5	70 ± 6	53 ± 6	38 ± 6
305 ± 5	449 ± 19	384 ± 15	274 ± 11	207 ± 9	144 ± 7	101 ± 6	81 ± 6	72 ± 6	62 ± 6	56 ± 7	34 ± 7

TABLE 2 (continued)

E_γ (MeV)	θ_p^{cm} (deg)										
	40°	50°	60°	70°	80°	90°	100°	110°	120°	130°	140°
315 ± 5	380 ± 19	359 ± 15	281 ± 12	196 ± 9	144 ± 8	103 ± 6	68 ± 6	51 ± 6	45 ± 6	45 ± 7	35 ± 7
325 ± 5	343 ± 17	308 ± 14	245 ± 11	188 ± 9	124 ± 7	83 ± 6	61 ± 6	66 ± 6	56 ± 6	48 ± 6	40 ± 8
335 ± 5	366 ± 19	302 ± 15	225 ± 11	151 ± 8	127 ± 7	84 ± 6	70 ± 6	54 ± 5	48 ± 6	48 ± 7	43 ± 8
345 ± 5	330 ± 16	267 ± 12	192 ± 9	137 ± 7	110 ± 6	70 ± 5	66 ± 5	47 ± 5	45 ± 5	43 ± 6	34 ± 7
355 ± 5	263 ± 17	240 ± 14	158 ± 10	138 ± 8	82 ± 6	59 ± 5	60 ± 6	57 ± 6	38 ± 6	39 ± 7	26 ± 7
365 ± 5	260 ± 17	225 ± 14	151 ± 10	125 ± 8	75 ± 6	59 ± 6	59 ± 5	48 ± 6	35 ± 6	27 ± 7	19 ± 6
375 ± 5	260 ± 17	219 ± 13	135 ± 10	102 ± 8	84 ± 7	62 ± 5	49 ± 5	46 ± 6	41 ± 6	35 ± 7	11 ± 7
385 ± 5	210 ± 16	175 ± 12	133 ± 9	106 ± 8	75 ± 6	44 ± 5	44 ± 5	35 ± 5	34 ± 6	37 ± 7	30 ± 8
395 ± 5	201 ± 15	169 ± 11	104 ± 8	86 ± 7	62 ± 5	37 ± 4	37 ± 4	33 ± 5	32 ± 5	31 ± 6	36 ± 7
410 ± 10	170 ± 11	149 ± 8	85 ± 6	67 ± 5	56 ± 4	42 ± 3	32 ± 3	33 ± 3	26 ± 4	26 ± 4	22 ± 5
430 ± 10	135 ± 9	114 ± 7	79 ± 5	52 ± 3	39 ± 3	31 ± 3	30 ± 3	24 ± 3	19 ± 3	18 ± 4	15 ± 4
450 ± 10	115 ± 10	99 ± 8	70 ± 6	37 ± 4	28 ± 3	24 ± 3	28 ± 3	20 ± 3	15 ± 3	16 ± 4	12 ± 5
470 ± 10	108 ± 9	76 ± 7	58 ± 5	37 ± 4	23 ± 3	18 ± 2	18 ± 2	13 ± 3	14 ± 3	10 ± 3	12 ± 4

TABLE 2 (continued)

E_γ (MeV)	θ_p^{cm} (deg)										
	40°	50°	60°	70°	80°	90°	100°	110°	120°	130°	140°
490 ± 510	89 ± 9	70 ± 6	41 ± 4	26 ± 3	18 ± 3	15 ± 2	15 ± 2	13 ± 3	13 ± 3	14 ± 3	9 ± 4
525 ± 25	65 ± 5	41 ± 3	24 ± 2	20 ± 2	12.1 ± 1.4	8.1 ± 1.2	12.1 ± 1.5	12.0 ± 1.5	10.0 ± 1.9	6.9 ± 1.7	2.6 ± 2.1
575 ± 25	37 ± 4	32 ± 3	19 ± 2	7.9 ± 1.4	4.7 ± 1.1	3.3 ± 1.0	4.4 ± 1.1	5.6 ± 1.3	6.4 ± 1.5	5.7 ± 2.0	2.8 ± 3.0
625 ± 25	26 ± 4	17 ± 3	9.7 ± 1.7	4.9 ± 1.2	3.5 ± 0.9	1.5 ± 0.8	2.0 ± 1.0	4.2 ± 1.2	2.0 ± 1.3	4.2 ± 1.6	2.6 ± 2.4
675 ± 50	20 ± 4	12 ± 2	4.9 ± 1.5	2.3 ± 0.8	0.7 ± 0.7	0.8 ± 0.7	2.0 ± 1.0	1.9 ± 0.9	2.7 ± 1.3	3.8 ± 2.6	5.6 ± 2.3
750 ± 50	9.9 ± 1.9	5.6 ± 1.3	2.7 ± 0.8	0.5 ± 0.5	1.4 ± 0.4	0.1 ± 0.3	1.0 ± 0.5	1.9 ± 0.8	2.3 ± 0.8	2.8 ± 1.4	0.6 ± 1.1

FIG. 1

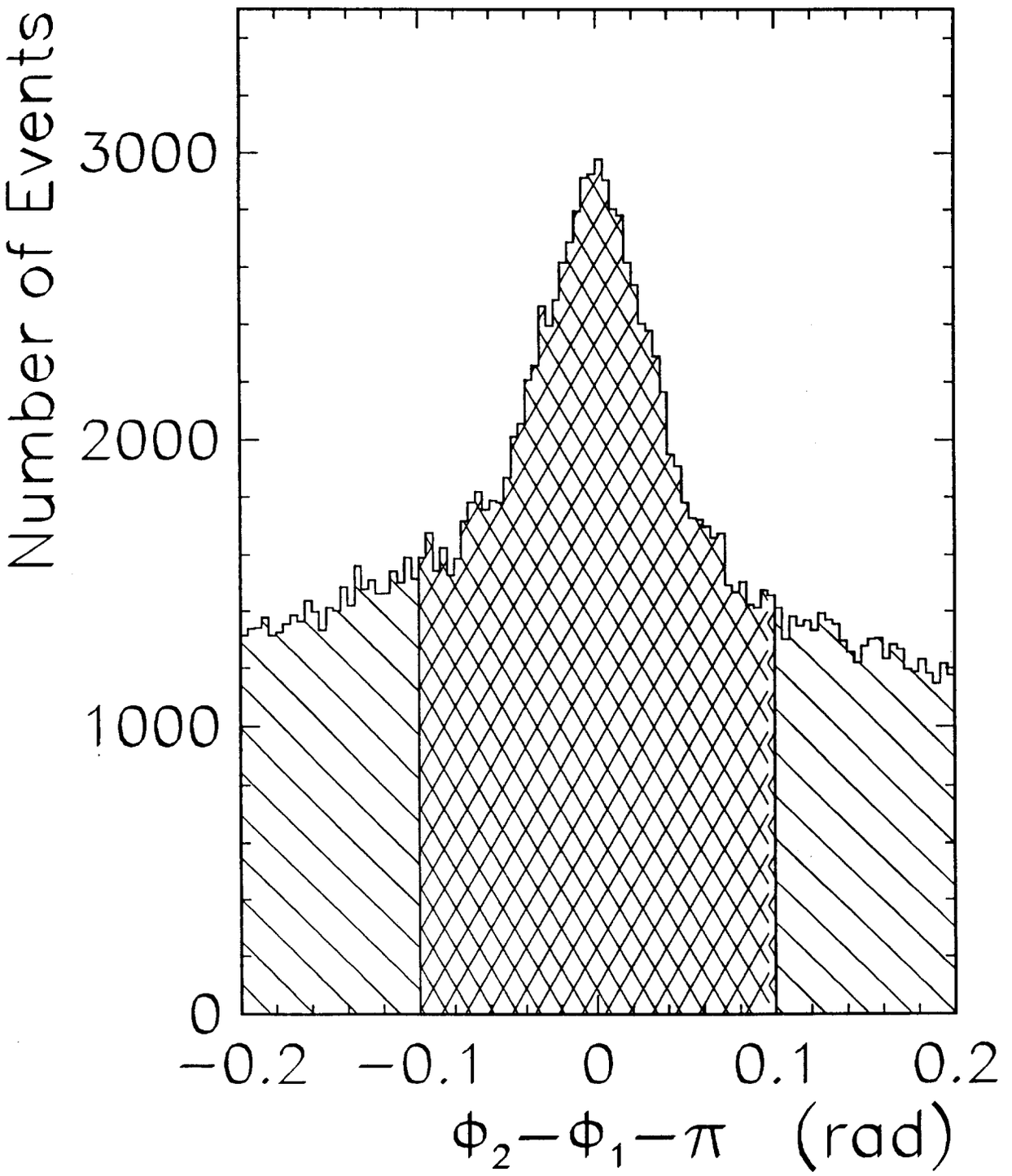

FIG. 2

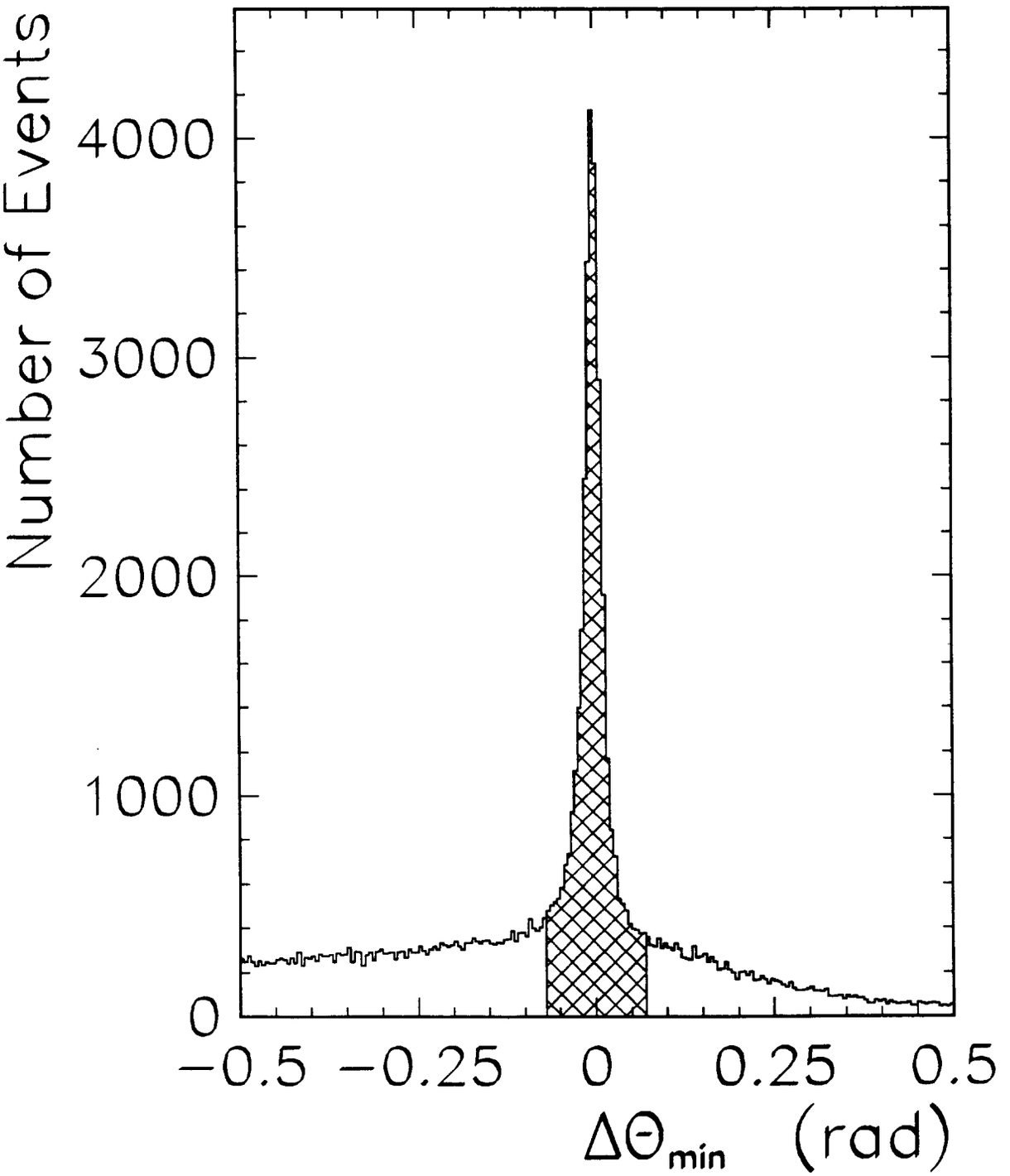
Number of Events
4000
3000
2000
1000
0
−0.5
−0.25
0
0.25
0.5
ΔΘmin (rad)

FIG. 3

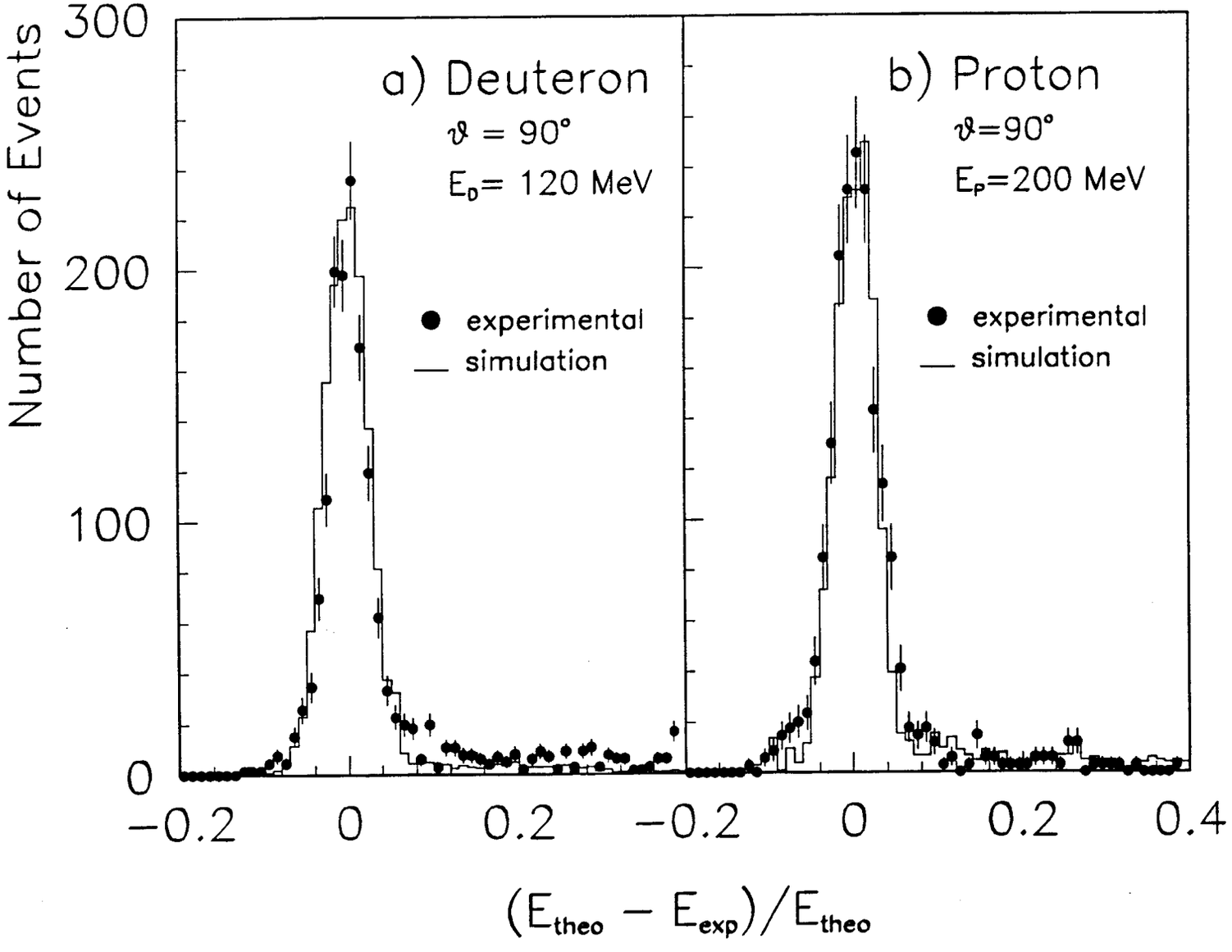
Number of Events
300
200
100
0
a) Deuteron
ϑ = 90°
E_D= 120 MeV
experimental
simulation
b) Proton
ϑ=90°
E_P=200 MeV
experimental
simulation
−0.2
0
0.2
−0.2
0
0.2
0.4
(E_theo − E_exp)/E_theo

FIG. 4

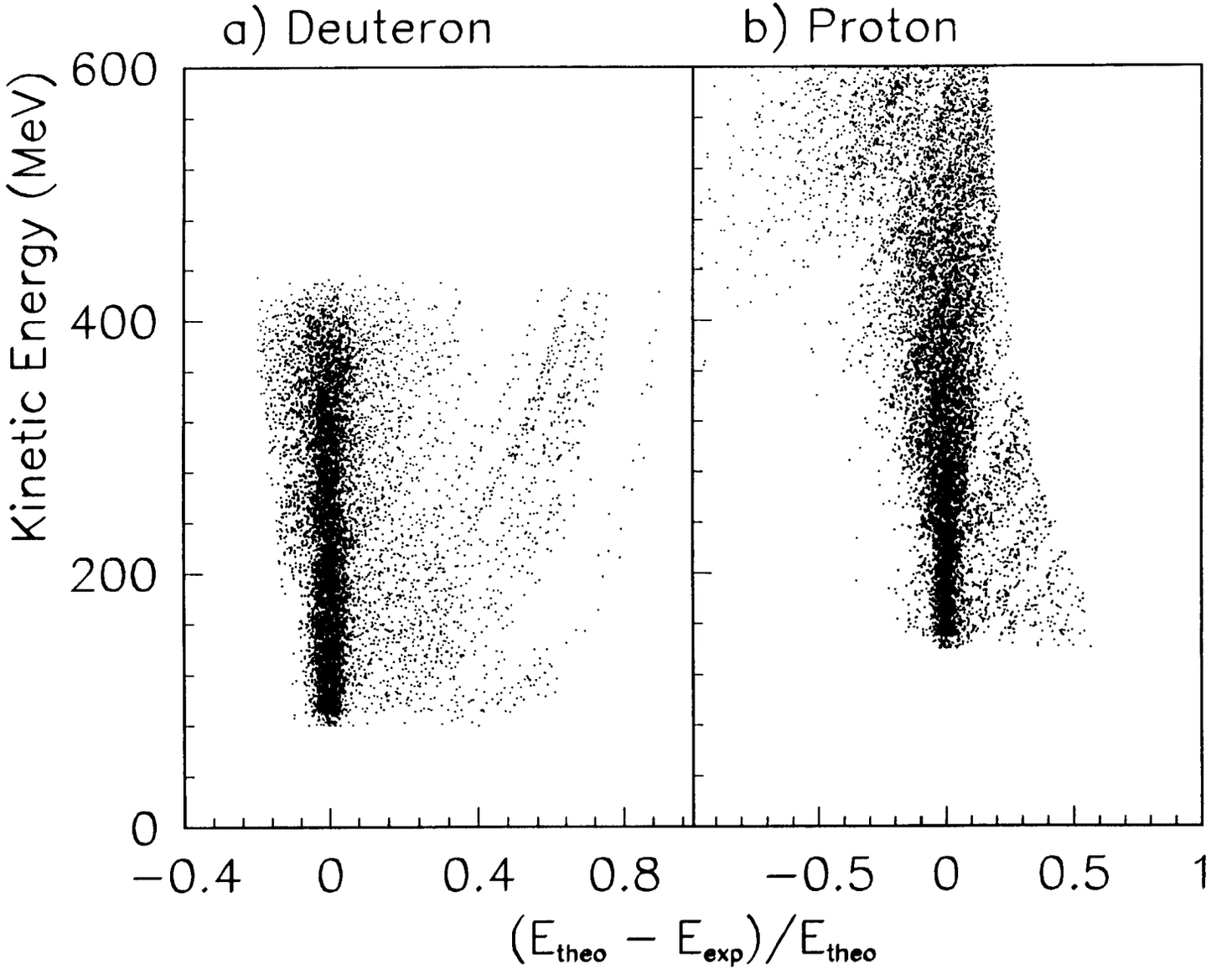
a) Deuteron
b) Proton
Kinetic Energy (MeV)
600
400
200
0
−0.4
0
0.4
0.8
−0.5
0
0.5
1
$(E_{theo} - E_{exp})/E_{theo}$

FIG. 5

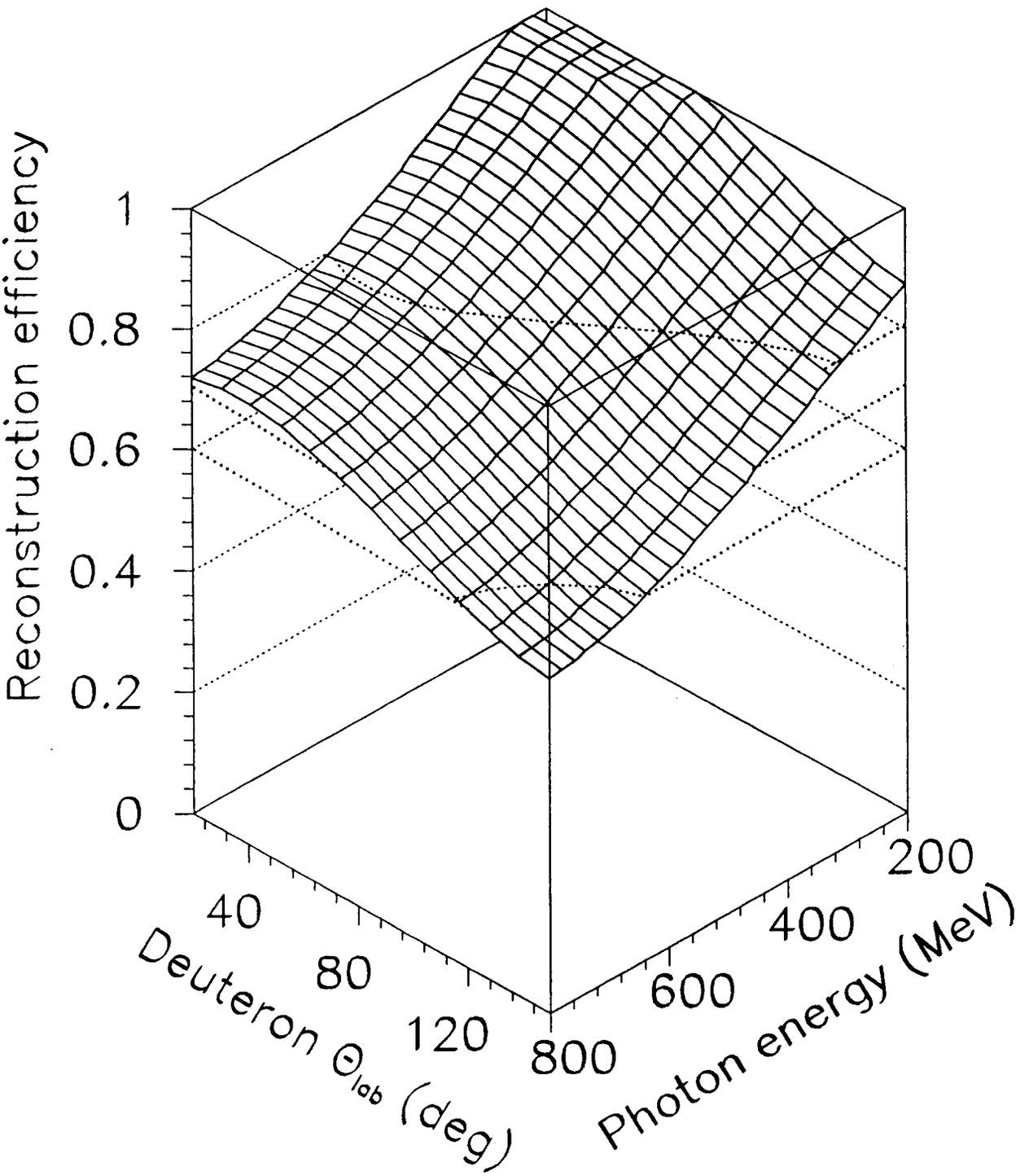
Reconstruction efficiency
1
0.8
0.6
0.4
0.2
0
40
80
120
800
Deuteron Θ_{lab} (deg)
200
400
600
Photon energy (MeV)

FIG. 6

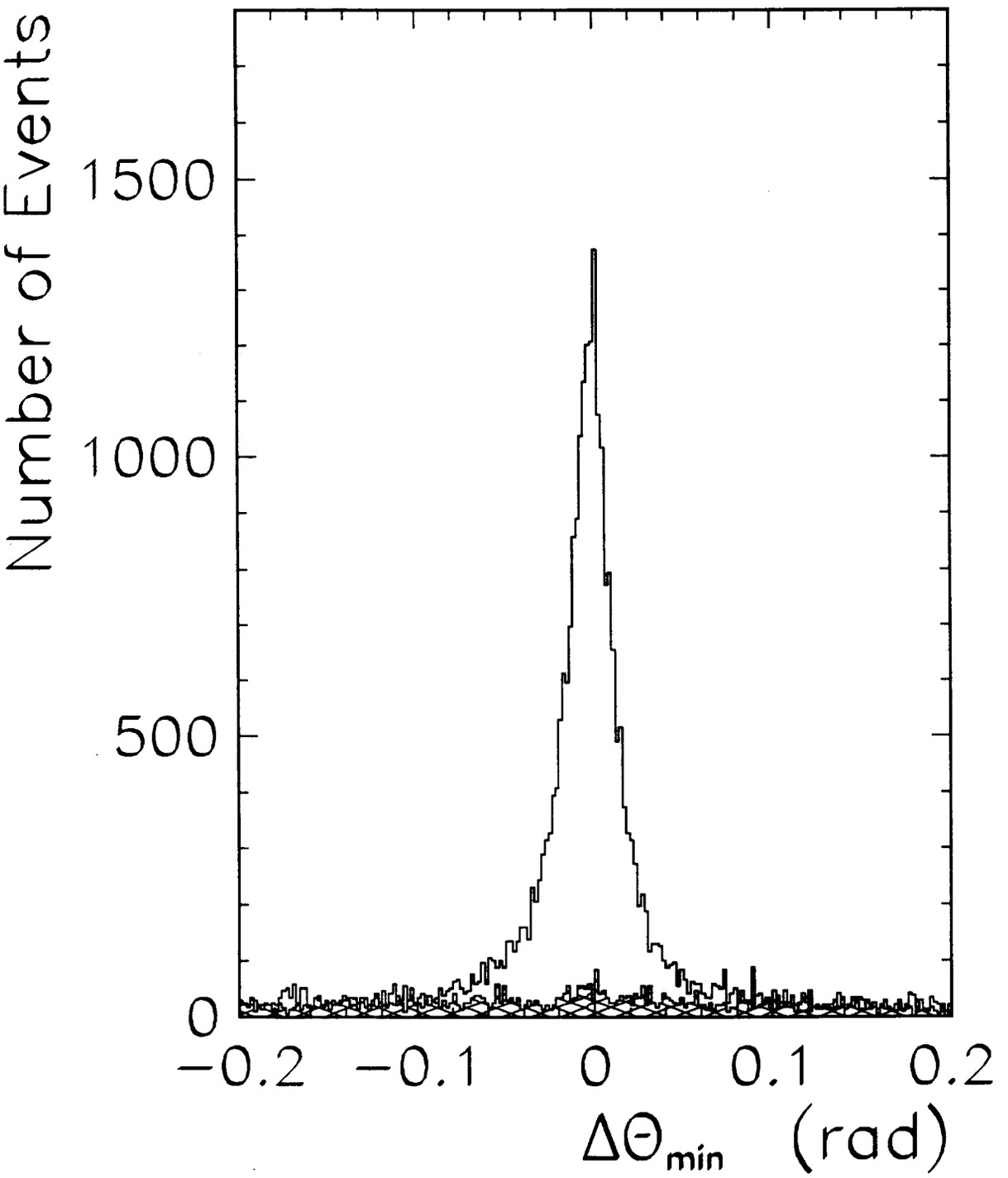

FIG. 7

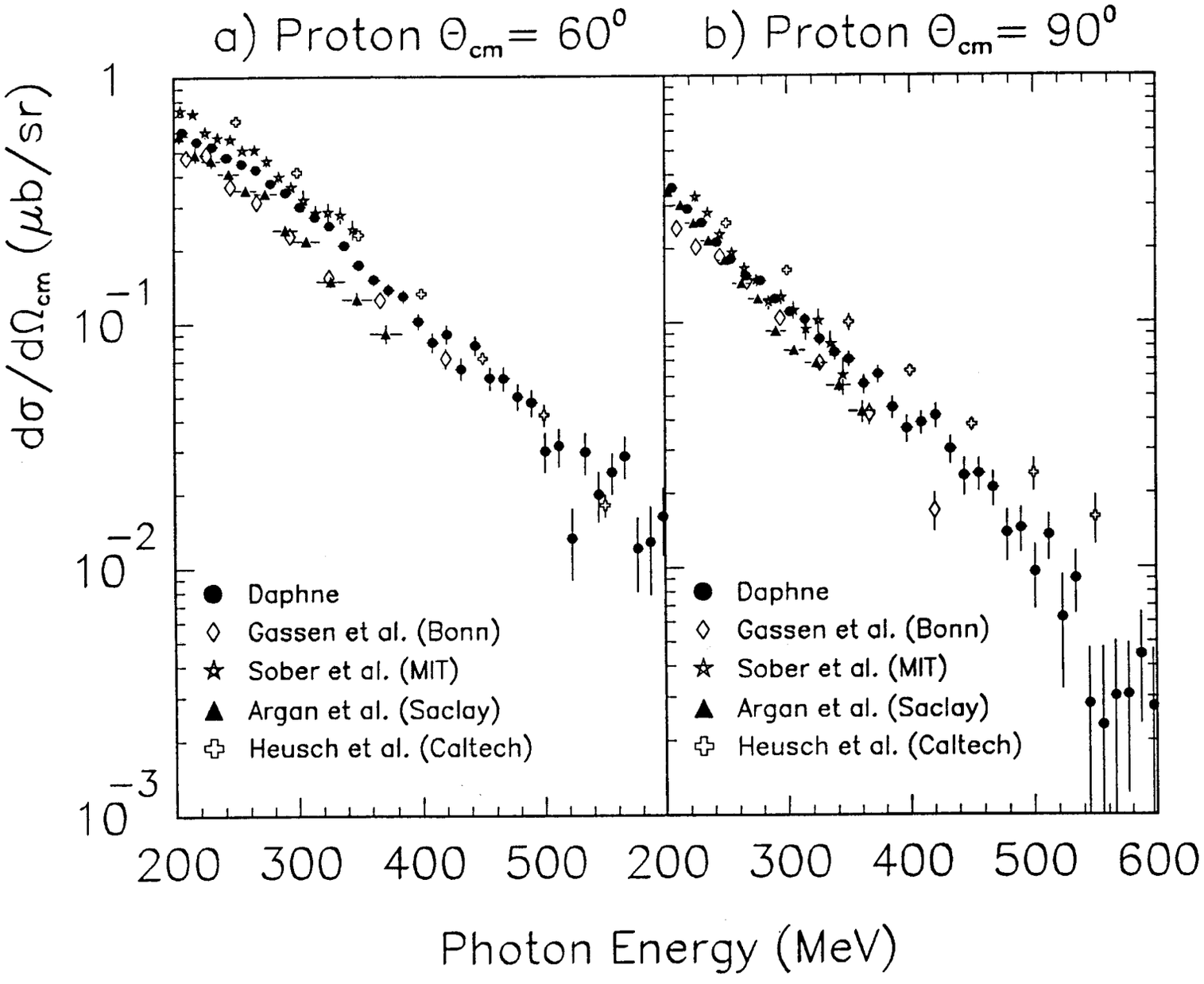
a) Proton Θ_{cm}= 60°
b) Proton Θ_{cm}= 90°
$d\sigma/d\Omega_{cm}$ (μb/sr)
1
10^{-1}
10^{-2}
10^{-3}
Daphne
Gassen et al. (Bonn)
Sober et al. (MIT)
Argan et al. (Saclay)
Heusch et al. (Caltech)
200 300 400 500 200 300 400 500 600
Photon Energy (MeV)

FIG. 8

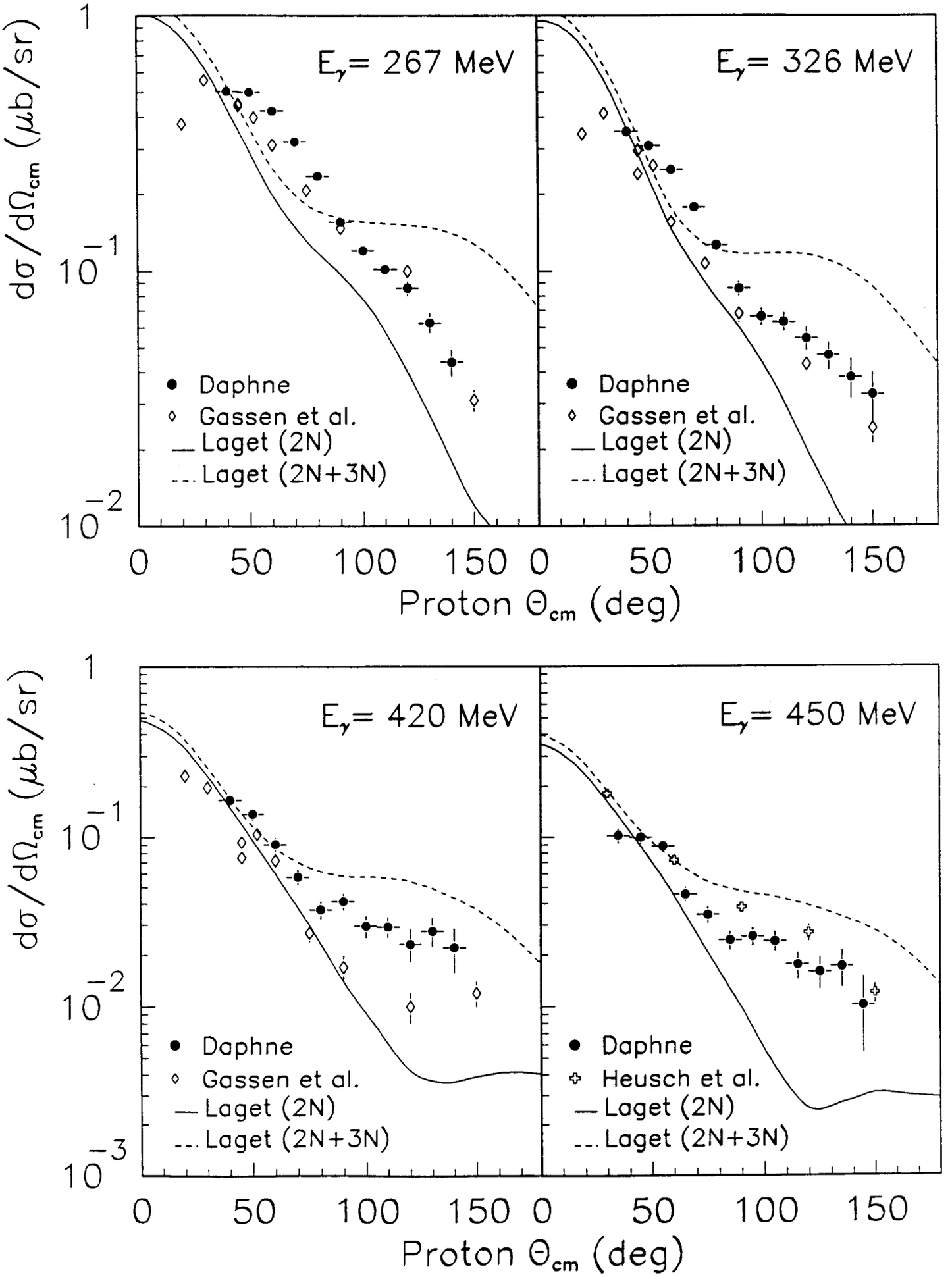
E_γ= 267 MeV
E_γ= 326 MeV
E_γ= 420 MeV
E_γ= 450 MeV
Daphne
Gassen et al.
Heusch et al.
Laget (2N)
Laget (2N+3N)
$d\sigma/d\Omega_{cm}$ (μb/sr)
Proton Θ_{cm} (deg)
1
10^{-1}
10^{-2}
10^{-3}
0
50
100
150

FIG. 8 (continued)

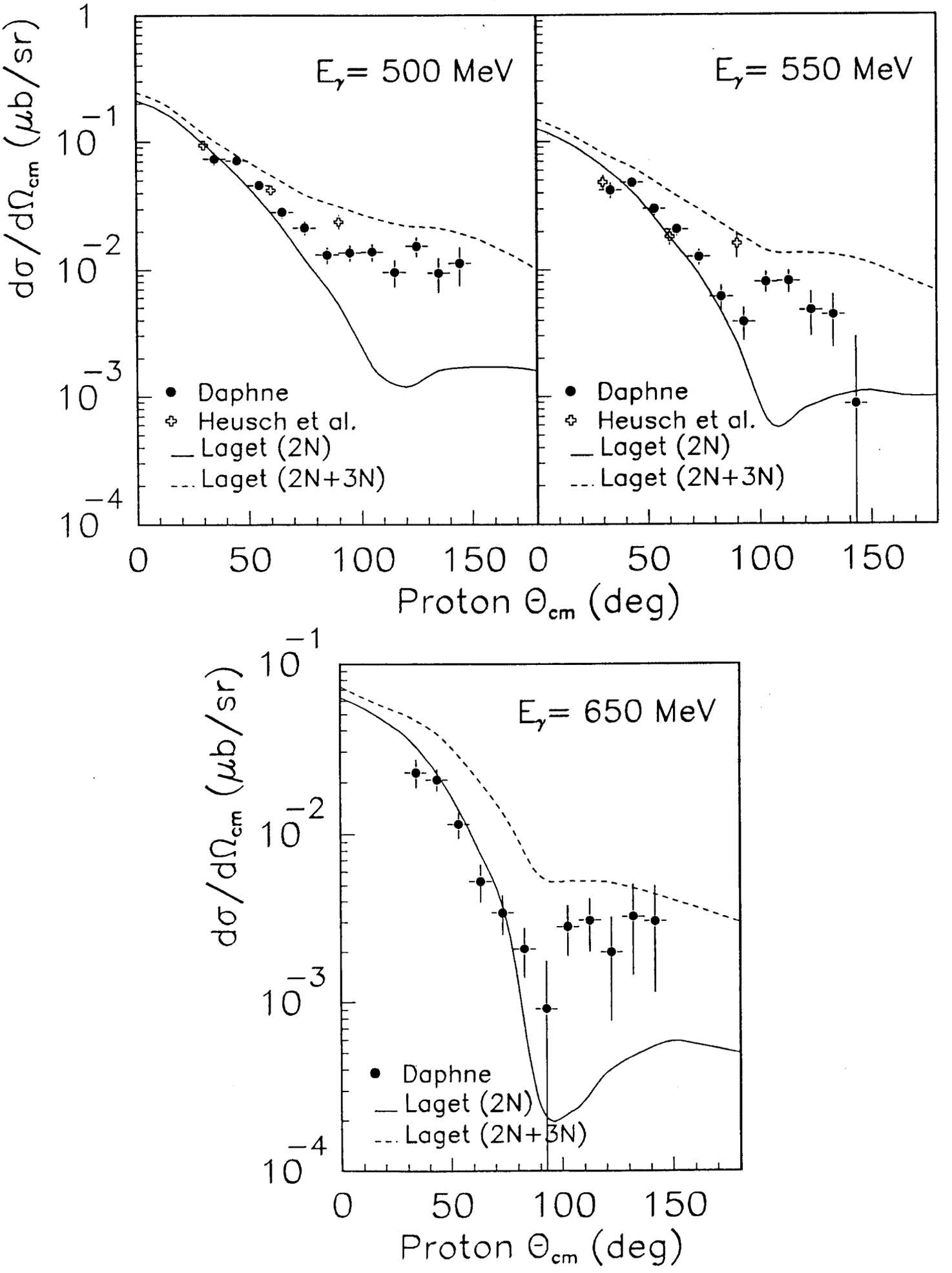

FIG. 9

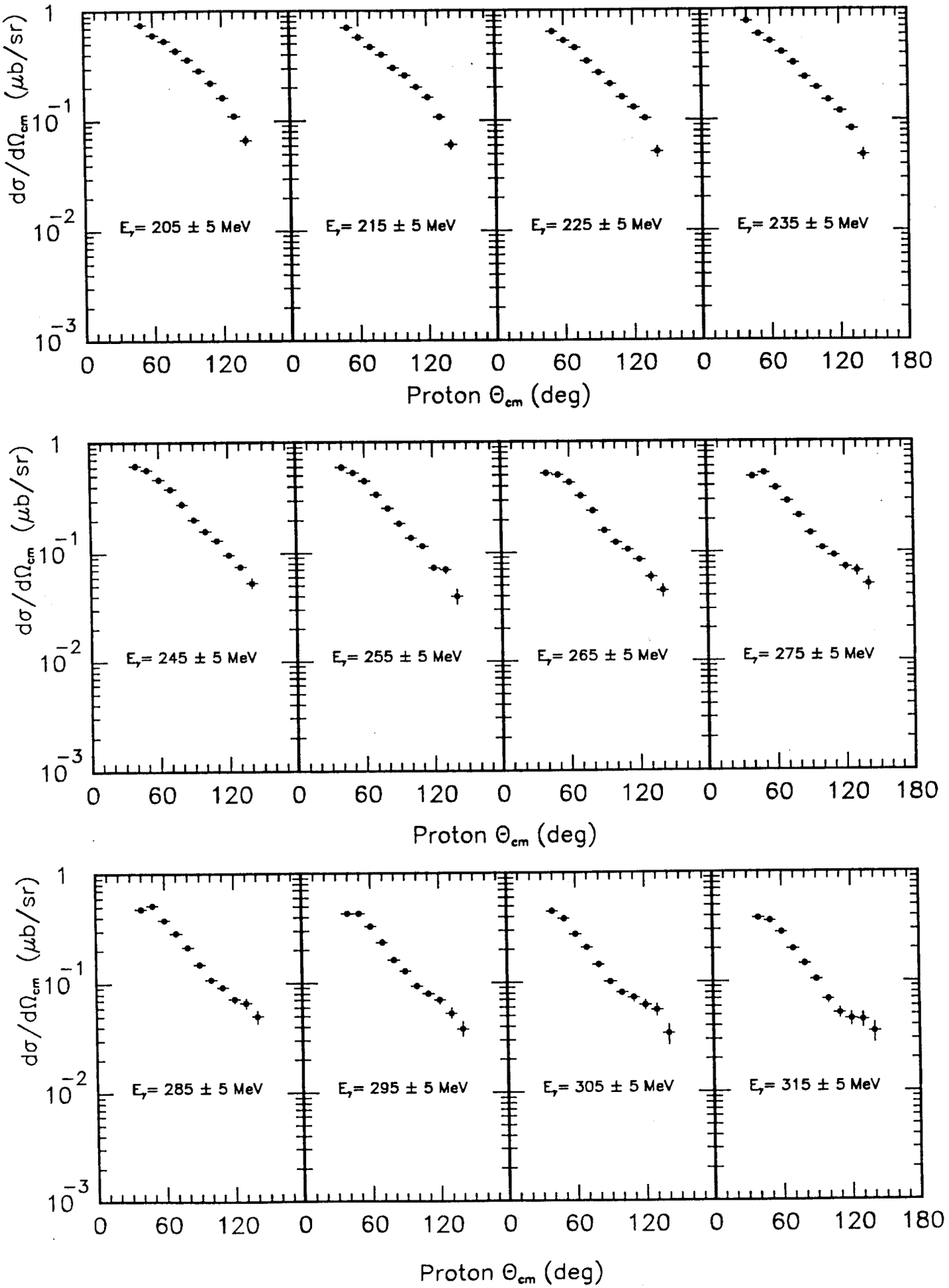
dσ/dΩcm (μb/sr)
1
10⁻¹
10⁻²
10⁻³
Eγ= 205 ± 5 MeV
Eγ= 215 ± 5 MeV
Eγ= 225 ± 5 MeV
Eγ= 235 ± 5 MeV
Eγ= 245 ± 5 MeV
Eγ= 255 ± 5 MeV
Eγ= 265 ± 5 MeV
Eγ= 275 ± 5 MeV
Eγ= 285 ± 5 MeV
Eγ= 295 ± 5 MeV
Eγ= 305 ± 5 MeV
Eγ= 315 ± 5 MeV
0
60
120
180
Proton Θcm (deg)

FIG. 9 (continued)

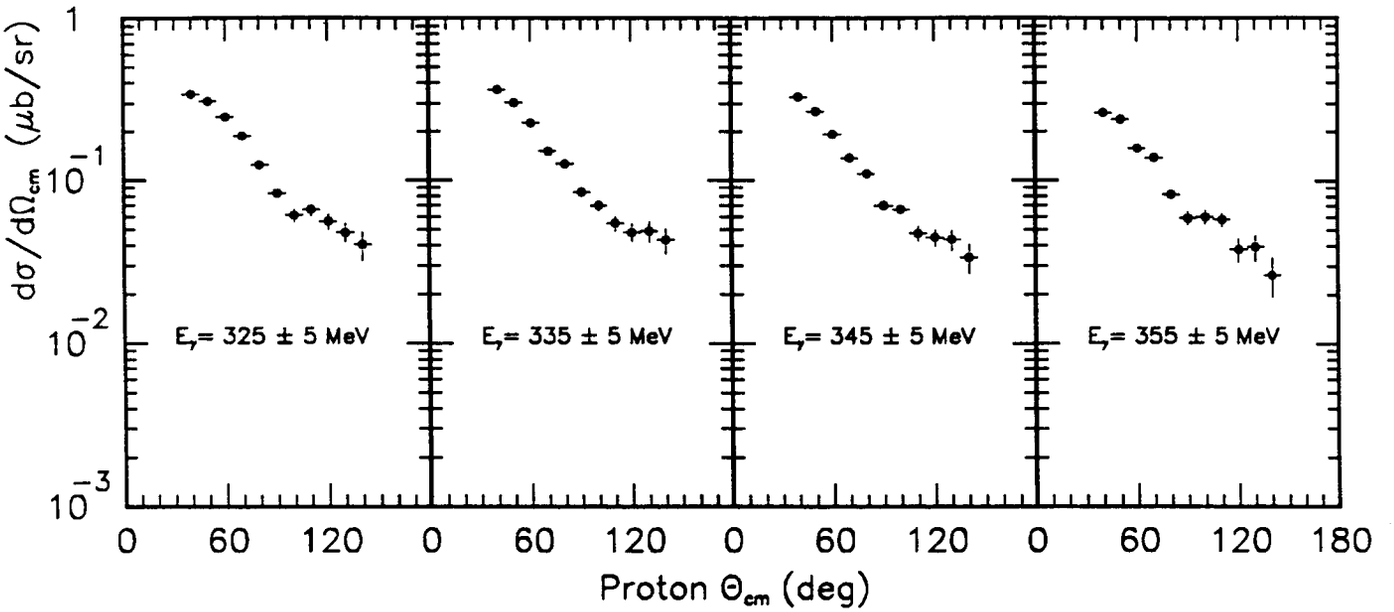

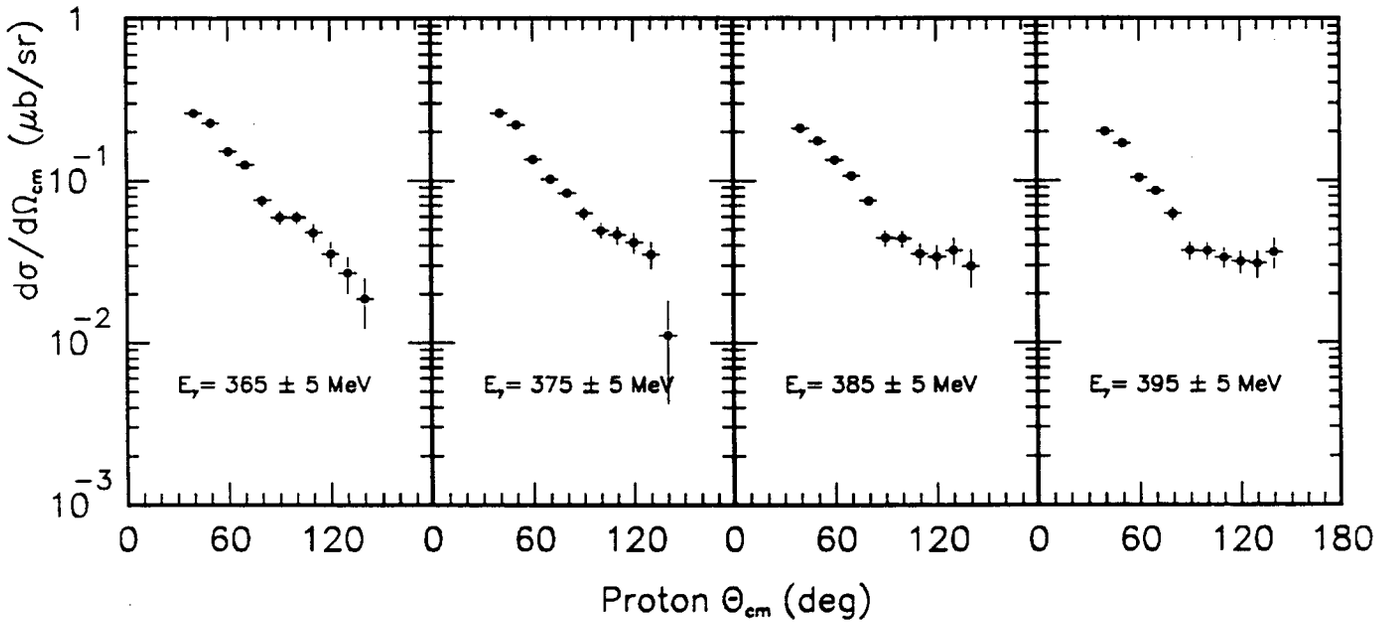

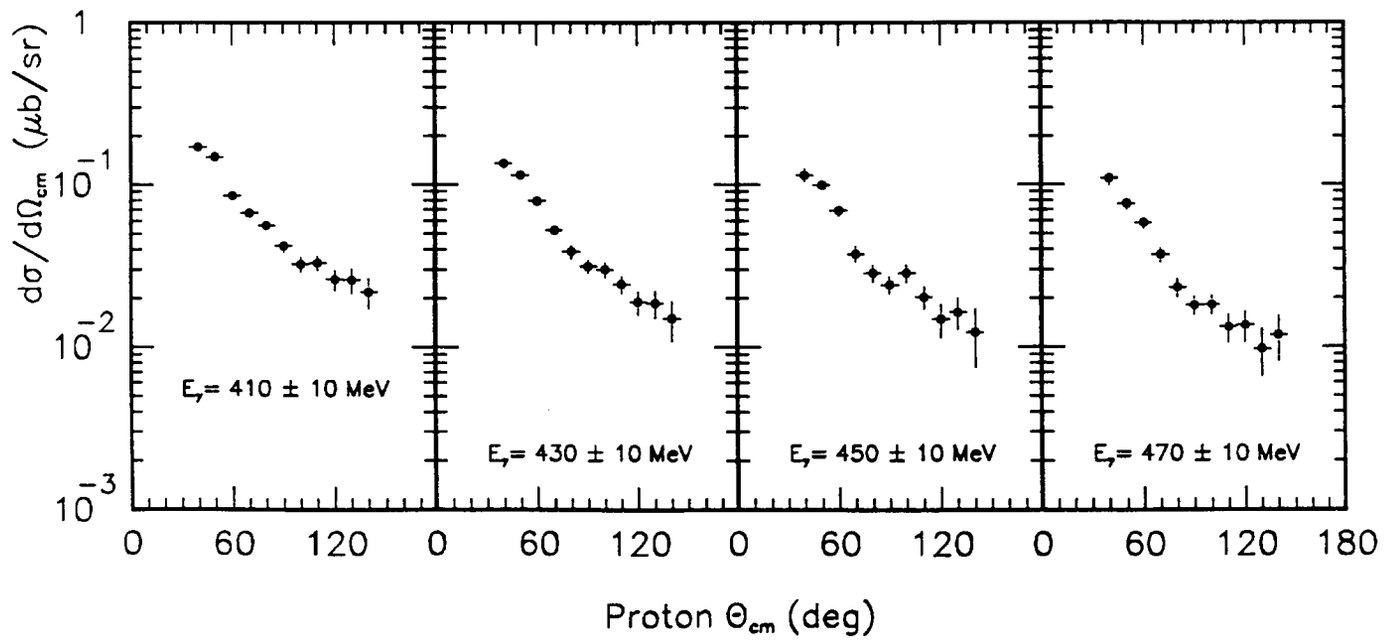

FIG. 9 (continued)

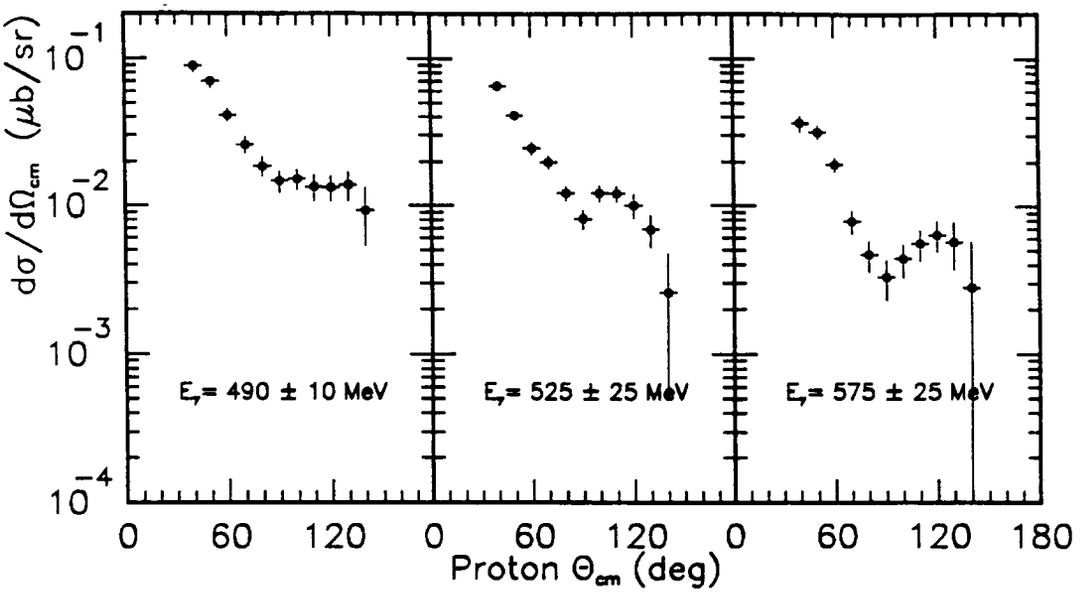

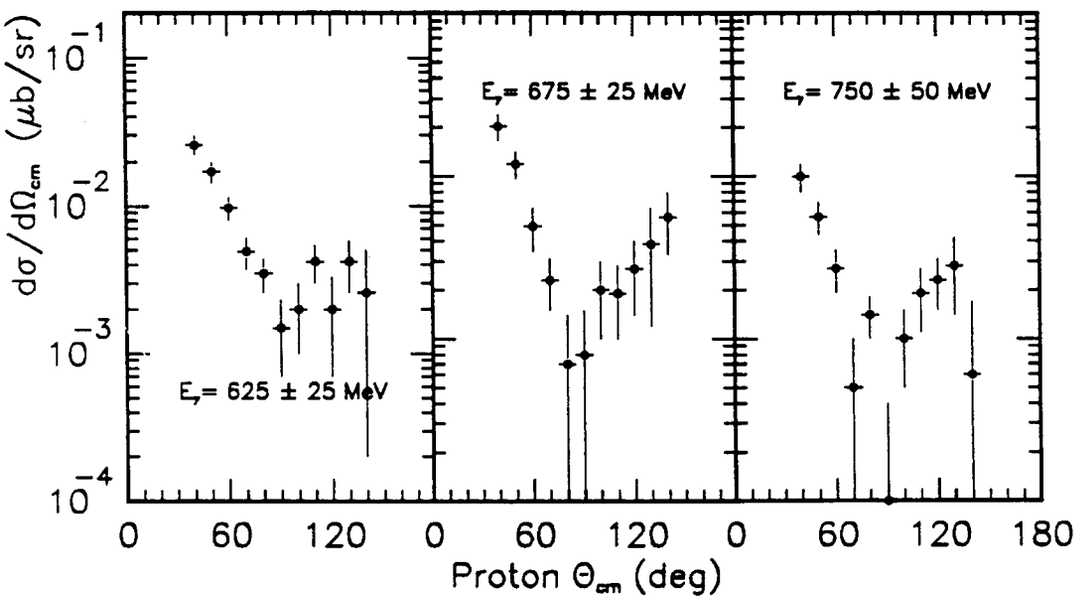

FIG. 10